POLITECNICO DI TORINO
Repository ISTITUZIONALE

Electrochemical Characterization of Flexible Interdigitated Electrodes for Hydration Monitoring

Original
Electrochemical Characterization of Flexible Interdigitated Electrodes for Hydration Monitoring / Iannucci, L., Longombardo, S.R., Lombardo, L., Parvis, M., Tonello, S., Galli, A., Grassini, S.. - ELETTRONICO. - (2023), pp. 1-6. (2023 IEEE International Symposium on Medical Measurements and Applications (MeMeA) Jeju (KOR) 14-16 June 2023) [10.1109/MeMeA57477.2023.10171901].

Availability:
This version is available at: 11583/2981183 since: 2023-08-22T12:22:31Z

Publisher:
IEEE

Published
DOI:10.1109/MeMeA57477.2023.10171901

Terms of use:

This article is made available under terms and conditions as specified in the corresponding bibliographic description in the repository

Publisher copyright
IEEE postprint/Author's Accepted Manuscript

©2023 IEEE. Personal use of this material is permitted. Permission from IEEE must be obtained for all other uses, in any current or future media, including reprinting/republishing this material for advertising or promotional purposes, creating new collecting works, for resale or lists, or reuse of any copyrighted component of this work in other works.

(Article begins on next page)

19 November 2026

Electrochemical characterization of flexible interdigitated electrodes for hydration monitoring

Leonardo Iannucci
Department of Applied Science and Technology
Politecnico di Torino
Turin, Italy
leonardo.iannucci@polito.it

Sofia Rita Longombardo
Department of Applied Science and Technology
Politecnico di Torino
Turin, Italy
sofiarita.longombardo@studenti.polito.it

Luca Lombardo
Department of Electronics and Telecommunication
Politecnico di Torino
Turin, Italy
luca.lombardo@polito.it

Marco Parvis
Department of Electronics and Telecommunication
Politecnico di Torino
Turin, Italy
marco.parvis@polito.it

Sarah Tonello
Department of Information Engineering
University of Padova
Padova, Italy
sarah.tonello@unipd.it

Alessandra Galli
Department of Information Engineering
University of Padova
Padova, Italy
alessandra.galli@unipd.it

Sabrina Grassini
Department of Applied Science and Technology
Politecnico di Torino
Turin, Italy
sabrina.grassini@polito.it

***Abstract*—The use of flexible interdigitated electrodes has increased significantly over the last years thanks to the development and optimization of innovative production techniques which allow to realise tailored sensors geometries. Actually, interdigitated geometry improves the measurement sensitivity and allows to use small sample volumes. This is of particular interest in biomedical applications, where the possibility to have a substrate that conforms to the body is crucial to obtain reliable results. In this context, impedimetric sensors can offer important applications both in measuring analytes concentration and in monitoring skin hydration, a medical parameter of paramount importance for many patients. The development of wearable sensors can open new possibilities in the field of telemedicine to monitor patients also outside of the hospitals and thus to prevent critical situations. This study provides a comprehensive electrochemical characterization of flexible interdigitated electrodes produced by inkjet printing. The cell constant value is computed by experimental measurements in saline solutions and then their use for hydration monitoring by impedance measurements is shown by in-vitro experiments using agar gel samples. The use of equivalent electrical circuits to model the experimental data allowed to fully describe the electrochemical system, identifying the frequency ranges which are relevant for the proposed application.**

***Index Terms*—Electrochemical Impedance Spectroscopy, Interdigitated electrodes, Hydration monitoring, Impedimetric sensors**

I. Introduction

Hydration level in human body is one of the most important physiological parameters, which allows clinicians to quickly assess the overall conditions of a patient [1]. Actually, insufficient hydration can be indicative of faults in kidney functionality or diabetes and may affects heart rate (due to low blood pressure). Even when not related to any disease, it is important to keep a good hydration level in order to mantain the correct equilibrium of electrolytes and metabolites. Actually water content allows regulating different physiological parameters such as the body temperature and the blood pressure [2]. In this context, elderly people generally have more difficulties in keeping a good hydration level, due to reduced sense of thirst and because the total amount of water in their body is naturally lower respect to young people [3]. For this reason, it is really important to develop new solutions of telemedicine able to continuously monitor the hydration level, giving alarms in case of need.

Over the last years, many devices have been developed, based on wearable sensors [4]. Generally, the focus is on the measure of analytes of interest such as glucose, lactate and ions (sodium and potassium in particular) and on the assessment of the hydration level [4]–[7]. The latter can be investigated by monitoring the dielectric characteristics of the skin using Electrochemical Impedance Spectroscopy (EIS) [8], [9]. Actually, this technique offers many advantages, being non-invasive and based on the application of a small electrical stimulus. Thanks to its relative simplicity, many portable and low-cost instruments have been developed, which can be integrated in a wearable device to perform impedance analyses [10]–[13]. As far as the sensor geometry is concerned, interdigitated sensors are generally the most common because they provide high sensitivity even with small sample size [14]. Their use has been extensively demonstrated for different analytes and many studies have investigated the best geometries to increase sensors performance [8], [15]. Ibrahim et al. [16] demonstrated that sensitivity is improved by choosing a spacing between interdigitated fingers that is two thirds of the finger width. Orazem et al. [17] showed the influence of interdigitated geometry on the current distribution and thus on the measured impedance. As far as the specific applica-

tion of hydration monitoring is concerned, Yao et al. [18] showed the possible use of a wristband based on interdigitated sensors made of silver nanowires in a polydimethylsiloxane matrix. The researchers found a good correlation between the measured impedance characteristics of skin and the hydration level assessed by a commercial moisture meter, but, due to the limited investigated frequency range (from 10^4 Hz to 10^5 Hz), deriving a complete electrochemical model for the system was not straightforward. Matsukawa et al. [19] presented the results from the use of different interdigitated geometries (varying the spacing between digits) and focused on the possible inhibition of the water evaporation process due to the presence of the electrode itself. Results showed the good performance of the developed sensors, but, as the impedance measurement was acquired at a fixed frequency (i.e. 100 Hz), developing a complete model was not possible. For this reason, additional knowledge in this field can derive from the formulation of a model able to fully describe the system composed of the interdigitated sensor and the biological material.

Aim of this work is thus to provide a comprehensive characterization of flexible interdigitated sensors for hydration monitoring produced by ink-jet printing. The final goal is both to understand their electrochemical characteristics and, more importantly, to derive the proper model based on Equivalent Electrical Circuits. The interdigitated electrodes proposed were produced using the geometry optimised in previous studies, and then they were characterised in different saline solutions, to determine the cell constant of the interdigitated. Finally, as an in-vitro proof-of-concept, they were used to monitor by impedance spectroscopy measurements the water content in agar gel samples.

II. Materials and Methods

The interdigitated sensors were prepared using inkjet printing technology by means of the inkjet printer Dimatix DMP 2850 (FUJIFILM Dimatix, Inc., Santa Clara, California, USA). The substrate was a 30 μm-thick polymmide foil (Kapton, Dupont). The ink for sensors preparation was Sicrys^{TM} I40DM-106 (from PVNanocell, Israel), which is composed of silver nanoparticles suspended in diethylene glycol monomethyl ether (DGME). After printing, sensors were cured in an oven at the temperature of 250° C for 30 minutes, as recommended by the product datasheet. Before use, sensors were stored in a glove box, in order to avoid any contamination.

Sensors geometry was the same used in previous studies and it was chosen to optimise the transducing performances, thanks to an increased active surface area. The electrode fingers' dimensions were: length L = 9.0 mm, width W = 0.6 mm. Between each finger, a spacing S = 0.4 mm was present and all fingers of each electrode were connected to a collector having a width of 1.0 mm. The area of each interdigitated was equal to $0.557\ cm^2$.

EIS measurements were acquired using an IVIUM-n-Stat electrochemical interface. Impedance measurements were carried out in a two-electrode configuration, using a sinusoidal signal with 10 mV peak-amplitude. Measurements acquired in saline solutions were performed in the frequency range from 10^{-2} Hz to 10^5 Hz acquiring 10 points per frequency decade, while, to reduce the acquisition time, EIS measurements acquired on agar samples were limited to the frequency range from 10^{-1} Hz to 10^5 Hz, with 5 points per frequency decade.

EIS spectra were analysed also using Equivalent Electrical Circuit (EEC) modeling, by means of the IviumSoft software (Release 4.1038).

Aqueous saline solutions were prepared using KCl (potassium chloride) and deionised water. The following concentrations were prepared: 0.5 mM, 1.0 mM, 5.0 mM, and 10.0 mM. Solution resistivity was measured using a Mettler Toledo 'FiveEasy' Conductivity meter equipped with a LE703 probe.

The use of interdigitated electrodes to measure analytes concentration requires the calculation of the cell constant value (K_{cell}), which allows the user to scale the measured quantities in accordance to the electrode size and geometry [20]. This is related to the characteristic dimension (δ), expressed as [17]:

$$\delta = K_{cell} \cdot A \tag{1}$$

where A is the electrode area. In order to compute δ for the produced electrodes, in this study EIS measurements were acquired in different saline solutions containing increasing concentrations of KCl (as previously described). Actually, the characteristic dimension can be experimentally determined by the relation [15]:

$$\delta = \frac{dR_{sol}}{d\rho} \tag{2}$$

where R_{sol} is the measured solution resistance (expressed as $\Omega \cdot cm^2$) and ρ is the electrolyte resistivity (having unit of measurement $k\Omega \cdot cm$).

In-vitro tests for water-content monitoring were carried out using agar gel samples. Deionised water was mixed with agar powder (12 g/L) and KCl (0.7455 g/L), heated up to 90° C to obtain a homogenous solution, poured in plastic molds, and then let cool down to room temperature. After reaching room temperature and being solidified, agar samples were placed in a climatic chamber at 37°C and then removed regularly to be weighed and to acquire the EIS measurement. In this way, the loss of water in the agar samples was monitored both by gravimetric and electrochemical measurements.

All measurements were performed in triplicate.

III. Results and Discussion

A. Impedance measurements in saline solutions

The impedance measurements acquired in saline solutions at increasing KCl concentrations are presented in Figure 1 as Bode diagrams. As can be seen, all spectra exhibit a resistive behaviour in the high-frequency range, and then a capacitive-like behaviour at low frequencies. The breakpoint frequency (i.e. the frequency where the phase value reaches -45^o) falls between 10^0 Hz and 10^2 Hz for all sample solutions and it shifts towards higher frequencies increasing the electrolyte conductivity.

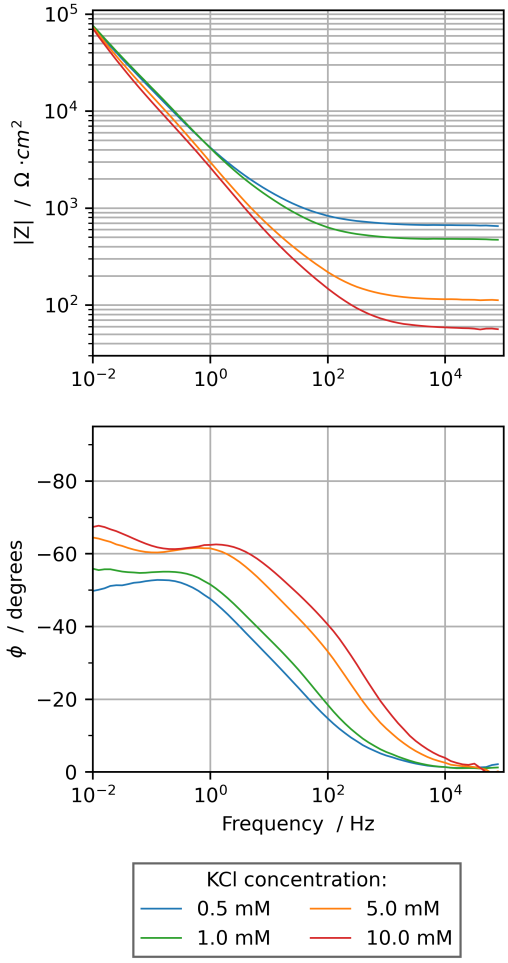


Fig. 1. Impedance spectra acquired in different KCl solutions.

In the high-frequency range, the impedance response is dominated by the effect of solution resistance and thus it decreases at higher electrolyte concentration. In the low-frequency range, impedance is mainly affected by the electrode-solution interface and it does not change significantly with KCl concentration.

In order to derive a physical model for the acquired spectra and then to compute the electrode cell constant, EIS data were fitted using equivalent electrical circuits (EEC). As all spectra were characterised by a single time constant, they were fitted using the circuit reported in Figure 2, which is composed by R0 (representing the solution resistance) in series to the parallel of a constant phase element (CPE1) and a resistor (R1). CPE1 and R1 model the interface between the electrode and the solution, i.e. the double-layer capacitance and the resistance to charge transfer respectively. The former was modeled by a CPE instead of a pure capacitor in order to take into account possible non-idealities and time-constant

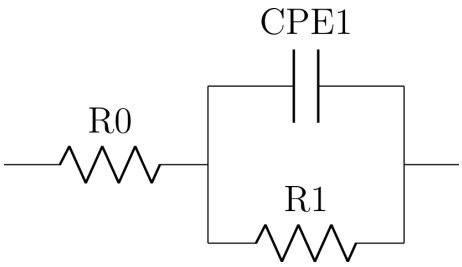


Fig. 2. Equivalent electrical circuit used to model the EIS spectra shown in Figure 1, acquired in saline solutions.

TABLE I
CIRCUIT PARAMETERS COMPUTED FOR THE EIS SPECTRA ACQUIRED IN SALINE SOLUTIONS (THE KCL CONCENTRATION IS REPORTED IN THE FIRST ROW). SEE FIGURE 2 FOR THE MEANING OF THE DIFFERENT ELEMENTS OF THE CIRCUIT.

Solution concentration:	0.5 mM	1 mM	5 mM	10 mM
R0 $[\Omega \cdot cm^2]$	$7.02 \cdot 10^2$	$4.89 \cdot 10^2$	$1.14 \cdot 10^2$	$5.7 \cdot 10^1$
R1 $[\Omega \cdot cm^2]$	$2.69 \cdot 10^5$	$6.40 \cdot 10^5$	$1.27 \cdot 10^6$	$7.47 \cdot 10^5$
Q1 $[s^\alpha/(\Omega \cdot cm^2)]$	$7.6 \cdot 10^{-5}$	$7.4 \cdot 10^{-5}$	$9.3 \cdot 10^{-5}$	$1.1 \cdot 10^{-4}$
$\alpha 1$	0.7	0.7	0.7	0.7
χ^2	$1.0 \cdot 10^{-2}$	$2.3 \cdot 10^{-2}$	$3.5 \cdot 10^{-3}$	$1.3 \cdot 10^{-2}$

dispersion [21]. The CPE impedance is defined as follows [22]:

$$Z_{CPE} = \frac{1}{(j\omega)^\alpha Q} \tag{3}$$

where j is the imaginary number, ω is the angular frequency, and Q and α are the CPE parameters. α ranges from 0 to 1; when it is equal to 1, Z_{CPE} represents the impedance of a pure capacitor, when it is equal to 0 it represents a resistor, while intermediate behaviour is observed for the other values.

All computed circuit parameters are reported in Table I.

The main changes in the circuit parameters were found to be in the R0 element, modeling the solution resistance. It decreases from $7.02 \cdot 10^2\ \Omega \cdot cm^2$ for the 0.5 mM KCl solution to $5.7 \cdot 10^1\ \Omega \cdot cm^2$ for the 10 mM KCl solution. As it was also observed from the graphical interpretation of the impedance spectra, R1, representing the charge transfer solution, does not exhibit relevant variations. Moreover, it is worth to notice that this circuit element is the one affected by the highest estimation uncertainty, because none of the spectra reaches the resistive plateaux at low frequency. Thus, the computed values are the result of an extrapolation and can not be directly derived from the experimental data. The CPE is slightly influenced by the electrolyte concentration. Actually, as shown in Table 1, Q1 increases going from 0.5 mM KCl to 10 mM KCl, while the parameter α remains stable at 0.7. Such a value for the CPE parameter is characteristic of a capacitance which is quite far from ideal behaviour, supporting the choice to use a CPE instead of an ideal capacitor.

The computation of the circuit parameters allows to determine the electrodes characteristic dimension (δ), as reported in Equation 2. The used procedure was the 'full-spectrum' method, as described in a previous publication [17]. Following

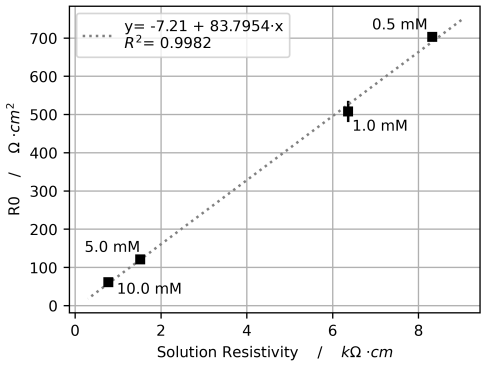


Fig. 3. Ohmic resistance (R0) plotted as a function of the solution resistivity to compute the electrodes' characteristic dimension δ.

this procedure, first the acquired spectrum is fitted using an appropriate EEC. After computing the EEC parameters, the ohmic impedance (R0) is estimated. So, for each electrolyte solution, this value is then plotted as a function of the solution resistivity, as shown in Figure 3. Indeed, δ is equal to the slope of the line interpolating the experimental points. In the characterised electrodes this is represented by the following equation:

$$y = -7.21 + 83.7954 \cdot x \tag{4}$$

which has a R^2 value of 0.9982. Therefore δ is equal to $838\ \mu m$. Dividing this value by the electrode area, it is finally possible to compute K_{cell}, which is equal to $0.150\ cm^{-1}$.

As previously said, this parameter is fundamental in any preliminary characterization of interdigitated electrodes because it allows scaling the measured quantities and thus deriving the actual concentration of a specific investigated analyte.

B. Impedance measurements on agar samples

A proof-of-concept for the use of the proposed inkjet printed sensors to monitor skin hydration was performed using agar samples. Actually, agar gel is often used in in-vitro studies to mimic human skin and tissues thanks to its dielectric characteristics, which are similar to biological material [23]–[25].

In the present study, agar samples were produced and then incubated in a climatic chamber at 37^oC. The weight loss, related to the water evaporation from the material, was monitored up to 180 min both by gravimetic and electrochemical measurements (EIS measurements acquired using the proposed sensors).

The trend of water evaporation is reasonably linear in the considered time-span ($R^2 = 0.9927$) and it allows to use this experimental setup to test the use of the sensors for hydration monitoring. EIS measurements were acquired after 10 minutes, 60 minutes, 120 minutes, and 180 minutes in the climatic chamber, i.e. after a weight loss equal to -1.8%, -5.7%, -9.4%, and -14.1%. The first spectrum was acquired after 10 minutes in the climatic chamber in order to have all

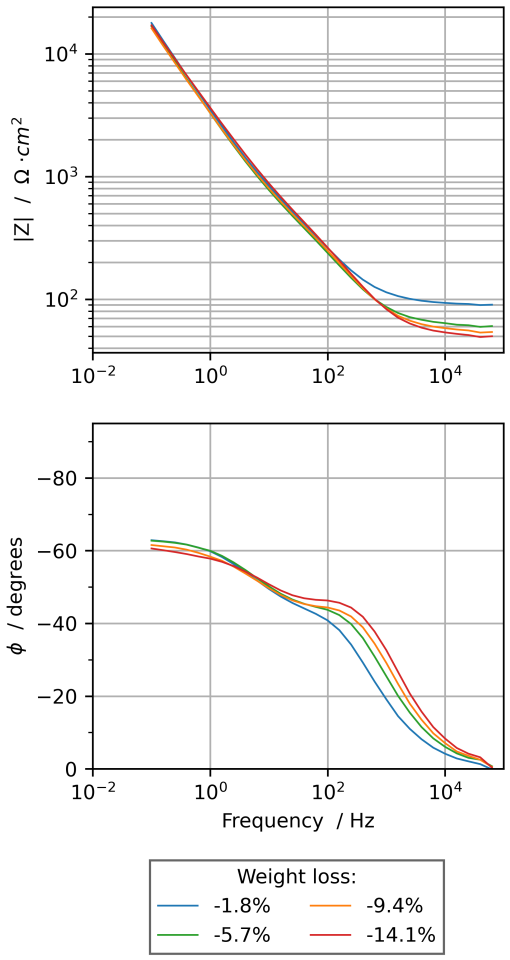


Fig. 4. Impedance spectra acquired on agar samples at different weight loss values.

measurements carried out at 37^oC (as EIS is deeply affected by the temperature).

EIS spectra acquired on agar samples are reported in Figure 4 as Bode diagrams.

As it can be seen both from the modulus and from the phase, the interdigitated sensors are able to detect a change in the impedance characteristics of the agar samples as a function of the water content. As far as the modulus is concerned, the values in the high-frequency part of the spectrum decrease while water molecules evaporate. In the low-frequency part, changes are almost not visible from graphical point of view. As far as the phase is concerned, two time constants are present in the graph, visible as two local maxima (the first centered at about 10^2 Hz and the second at about 10^{-1} Hz). Both peaks change their shape during the process of dehydration: the one at higher frequencies shifts and increases its height, while the one at lower frequencies slightly decreases its maximum.

In order to describe quantitatively the investigated system, the impedance spectra were modeled using an EEC. Taking

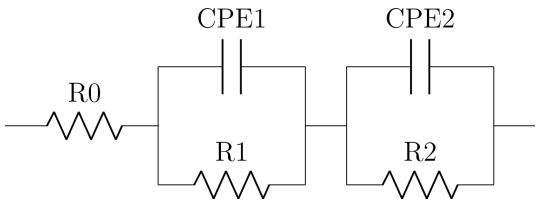


Fig. 5. Equivalent electrical circuit used to model the EIS spectra shown in Figure 4, acquired on agar samples.

TABLE II
CIRCUIT PARAMETERS COMPUTED FOR THE EIS SPECTRA ACQUIRED ON AGAR SAMPLES AT DIFFERENT WEIGHT LOSS VALUES (INDICATED IN THE FIRST ROW). SEE FIGURE 5 FOR THE MEANING OF THE DIFFERENT ELEMENTS OF THE CIRCUIT.

Weight loss:	-1.8%	-5.7%
R0 $[\Omega \cdot cm^2]$	$1.62 \cdot 10^2$	$1.07 \cdot 10^2$
R1 $[\Omega \cdot cm^2]$	$4.08 \cdot 10^2$	$3.78 \cdot 10^2$
Q1 $[s^{\alpha 1}/(\Omega \cdot cm^2)]$	$4.13 \cdot 10^{-5}$	$3.96 \cdot 10^{-5}$
$\alpha 1$	0.76	0.75
R2 $[\Omega \cdot cm^2]$	$1.31 \cdot 10^6$	$1.25 \cdot 10^6$
Q2 $[s^{\alpha 2}/(\Omega \cdot cm^2)]$	$4.40 \cdot 10^{-5}$	$4.69 \cdot 10^{-5}$
$\alpha 2$	0.72	0.72
χ^2	$5.36 \cdot 10^{-5}$	$8.12 \cdot 10^{-5}$
Weight loss:	-9.4%	-14.1%
R0 $[\Omega \cdot cm^2]$	$9.7 \cdot 10^1$	$8.8 \cdot 10^1$
R1 $[\Omega \cdot cm^2]$	$3.41 \cdot 10^2$	$3.11 \cdot 10^2$
Q1 $[s^{\alpha 1}/(\Omega \cdot cm^2)]$	$2.82 \cdot 10^{-5}$	$2.21 \cdot 10^{-5}$
$\alpha 1$	0.79	0.81
R2 $[\Omega \cdot cm^2]$	$1.11 \cdot 10^5$	$7.80 \cdot 10^5$
Q2 $[s^{\alpha 2}/(\Omega \cdot cm^2)]$	$4.81 \cdot 10^{-5}$	$4.30 \cdot 10^{-5}$
$\alpha 2$	0.70	0.70
χ^2	$1.62 \cdot 10^{-4}$	$6.63 \cdot 10^{-4}$

into account the two time constants present in all EIS spectra, the model shown in Figure 5 was chosen.

The EEC model is composed by the medium resistance (R0) and by the two RC in series. The former models the agar dielectric characteristics (R1 and CPE1) and influences the high-frequency part of the impedance spectrum, while the latter models the interface between the agar sample and the electrode (R2 and CPE2) and thus affects the low-frequency part of the spectrum. As already done in the previous EEC model, all capacitances have been modeled by constant phase elements.

The values for all computed parameters are reported in Table II.

Considering the physical interpretation of the EEC, the analysis can focus on R0, R1, Q1, and $\alpha 1$, which are the only parameters related to the dielectric characteristics of the agar. As it can be seen from Figure 6a, R0 has a decreasing trend, related to the fact that, while water evaporates from the material, KCl concentration increases and thus medium resistivity decreases accordingly. At the same time, a linear trend as a function of water loss was detected for R1 and Q1 (see Figure 6 b and c). The decrease in R1 can again be attributed to the increase in medium conductivity, while the medium capacitance (Q1) has a decreasing trend due to the loss of water from the agar. Similar trends were reported in

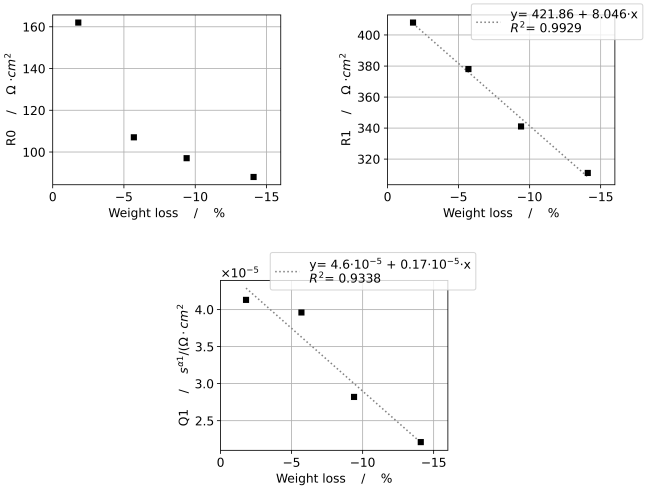


Fig. 6. Trend of the most important EEC parameters.

previous studies in which water absorption in organic materials was monitored [18], [26]. Actually, the high relative dielectric constant of water compared to organic material leads to a decrease in the measured capacitance during evaporation, due to the relation:

$$C = \frac{\epsilon_r \cdot \epsilon_0}{K_{cell}} \tag{5}$$

where ϵ_r is the material dielectric constant, and ϵ_0 is the permittivity in vacuum. Finally, as far as $\alpha 1$ is concerned, this parameter slightly increases its value during evaporation, going from 0.76 to 0.81.

The second time constant, modeled by R2 and Q2 and associated to the interface between the electrode and the agar sample, undergoes some fluctuations, which are not related to the change in hydration degree of the material and thus do not have a specific trend. As this part of the circuit is not physically related to the water evaporation, this does not have a particular significance for the performed study.

Thanks to the description of the system given by EECs, it is possible to conclude that the part of the spectrum which is relevant to monitor water loss is the one at high frequency and thus future measurements should focus only on this range.

IV. CONCLUSION

This study presented the electrochemical characterisation of inkjet-printed interdigitated electrodes, which can by useful for many biomedical applications. Actually, being realised on a flexible substrate, they can conform to the human body allowing to monitor analytes of interest or the hydration status of a patient.

In the present work, the cell parameter was estimated using impedance measurements in different saline solutions containing KCl. Then, as an in-vitro proof-of-concept, the water loss in agar gel samples was monitored as a function of the incubation time in a climatic chamber. The developed sensors were able to correctly detect the changes in the impedance characteristics of the agar samples related to the

water evaporation. Then, the presented modeling based on EEC allowed providing a comprehensive description of the investigated phenomena and thus a deeper understanding of the electrochemical system. In particular, it has been shown that the physical phenomena related to water evaporation from the organic material are visible in the high-frequency range of the investigated spectrum. This is of great interest for future applications in wearable sensors because it allows to significantly reduce the acquisition time. Indeed, considering the results obtained in this work, it would be possible to monitor skin dehydration acquiring only the impedance spectrum from 10 Hz to 10^5 Hz.

Future work will address further issues which must be taken into account for in-vivo tests, such as the stability of the sensing layer after contact with air and biological material (as fouling may occurr in these conditions [27]–[29]). Moreover, alternative strategies to process the acquired data and derive the estimation of the measured quantities will be investigated, such as chemiometrics and machine learning algorithms [30]–[32].

REFERENCES

[1] A. Samadi, T. Yazdanparast, M. Shamsipour, H. Hassanzadeh, M. Hashemi Orimi, R. Firooz, and A. Firooz, "Stratum corneum hydration in healthy adult humans according to the skin area, age and sex: a systematic review and meta-analysis," *Journal of the European Academy of Dermatology and Venereology*, vol. 36, no. 10, pp. 1713–1721, 2022.

[2] A. M. El-Sharkawy, O. Sahota, R. J. Maughan, and D. N. Lobo, "The pathophysiology of fluid and electrolyte balance in the older adult surgical patient," *Clinical Nutrition*, vol. 33, no. 1, pp. 6–13, 2014.

[3] S. P. Allison and D. N. Lobo, "Fluid and electrolytes in the elderly," *Current opinion in clinical nutrition and metabolic care*, vol. 7, no. 1, pp. 27–33, 2004.

[4] Y. Liu, M. Pharr, and G. A. Salvatore, "Lab-on-skin: A review of flexible and stretchable electronics for wearable health monitoring," *ACS Nano*, vol. 11, no. 10, pp. 9614–9635, 2017.

[5] W. Gao, S. Emaminejad, H. Y. Y. Nyein, S. Challa, K. Chen, A. Peck, H. M. Fahad, H. Ota, H. Shiraki, D. Kiriya, D. . Lien, G. A. Brooks, R. W. Davis, and A. Javey, "Fully integrated wearable sensor arrays for multiplexed in situ perspiration analysis," *Nature*, vol. 529, no. 7587, pp. 509–514, 2016.

[6] T. Fapanni, E. Sardini, M. Serpelloni, and S. Tonello, "Nano-functionalized electrochemical sensors by aerosol jet printing," *IEEE Sensors Journal*, vol. 22, no. 22, pp. 21498–21507, 2022.

[7] M. Scarpetta, M. Spadavecchia, G. Andria, M. A. Ragolia, and N. Giaquinto, "Simultaneous measurement of heartbeat intervals and respiratory signal using a smartphone," in *2021 IEEE International Symposium on Medical Measurements and Applications, MeMeA 2021 - Conference Proceedings*, 2021.

[8] R. AlDisi, Q. Bader, and A. Bermak, "Hydration assessment using the bio-impedance analysis method," *Sensors*, vol. 22, no. 17, 2022.

[9] T. V. A. Westermann, V. R. Viana, C. Berto Junior, C. B. Detoni da Silva, E. L. S. Carvalho, and C. G. Pupe, "Measurement of skin hydration with a portable device (skinup® beauty device) and comparison with the corneometer®," *Skin Research and Technology*, vol. 26, no. 4, pp. 571–576, 2020.

[10] P. Arpaia, D. Cuneo, S. Grassini, F. Mancino, S. Minucci, N. Moccaldi, and I. Sannino, "A finite element model of abdominal human tissue for improving the accuracy in insulin absorption assessment: A feasibility study," *Measurement: Sensors*, vol. 18, 2021.

[11] L. E. Sebar, L. Iannucci, E. Angelini, S. Grassini, and M. Parvis, "Electrochemical impedance spectroscopy system based on a teensy board," *IEEE Transactions on Instrumentation and Measurement*, vol. 70, 2021.

[12] K. Musioł, M. Kampik, and M. Koszarny, "A new sampling-based four-terminal-pair digital impedance bridge," *Measurement: Sensors*, vol. 18, 2021.

[13] A. I. Sunny, M. Rahman, M. Koutsoupidou, H. Cano-Garcia, M. Thanou, W. Rafique, O. Lipscombe, P. Kassanos, I. Triantis, E. Kallos, and P. Kosmas, "Feasibility experiments to detect skin hydration using a bio-impedance sensor," in *Proceedings of the Annual International Conference of the IEEE Engineering in Medicine and Biology Society, EMBS*, pp. 6032–6035, 2019.

[14] A. Dizon and M. E. Orazem, "On the impedance response of interdigitated electrodes," *Electrochimica Acta*, vol. 327, 2019.

[15] R. de la Rica, C. Fernández-Sánchez, and A. Baldi, "Polysilicon interdigitated electrodes as impedimetric sensors," *Electrochemistry Communications*, vol. 8, no. 8, pp. 1239–1244, 2006.

[16] M. Ibrahim, J. Claudel, D. Kourtiche, and M. Nadi, "Geometric parameters optimization of planar interdigitated electrodes for bioimpedance spectroscopy," *Journal of Electrical Bioimpedance*, vol. 4, no. 1, pp. 13–22, 2013.

[17] A. Dizon and M. E. Orazem, "On experimental determination of cell constants for interdigitated electrodes," *Electrochimica Acta*, vol. 337, 2020.

[18] S. Yao, A. Myers, A. Malhotra, F. Lin, A. Bozkurt, J. F. Muth, and Y. Zhu, "A wearable hydration sensor with conformal nanowire electrodes," *Advanced Healthcare Materials*, vol. 6, no. 6, 2017.

[19] R. Matsukawa, A. Miyamoto, T. Yokota, and T. Someya, "Skin impedance measurements with nanomesh electrodes for monitoring skin hydration," *Advanced Healthcare Materials*, vol. 9, no. 22, 2020.

[20] W. Olthuis, W. Streekstra, and P. Bergveld, "Theoretical and experimental determination of cell constants of planar-interdigitated electrolyte conductivity sensors," *Sensors and Actuators: B.Chemical*, vol. 24, no. 1-3, pp. 252–256, 1995.

[21] M. Orazem, I. Frateur, B. Tribollet, V. Vivier, S. Marcelin, N. Pebere, A. Bunge, E. White, D. Riemer, and M. Musiani, "Dielectric properties of materials showing constant-phase-element (cpe) impedance response," *Journal of the Electrochemical Society*, vol. 160, no. 6, pp. C215–C225, 2013.

[22] M. Orazem and B. Tribollet, *Electrochemical Impedance Spectroscopy*. 2008.

[23] S. Yao, A. Myers, A. Malhotra, F. Lin, A. Bozkurt, J. F. Muth, and Y. Zhu, "A wearable hydration sensor with conformal nanowire electrodes," *Advanced Healthcare Materials*, vol. 6, no. 6, 2017.

[24] X. Huang, H. Cheng, K. Chen, Y. Zhang, Y. Zhang, Y. Liu, C. Zhu, S. . Ouyang, G. . Kong, C. Yu, Y. Huang, and J. A. Rogers, "Epidermal impedance sensing sheets for precision hydration assessment and spatial mapping," *IEEE Transactions on Biomedical Engineering*, vol. 60, no. 10, pp. 2848–2857, 2013.

[25] T. Yilmaz, R. Foster, and Y. Hao, "Broadband tissue mimicking phantoms and a patch resonator for evaluating noninvasive monitoring of blood glucose levels," *IEEE Transactions on Antennas and Propagation*, vol. 62, no. 6, pp. 3064–3075, 2014.

[26] M. Jang, H. . Kim, H. . Koo, and J. . So, "Textile-based wearable sensor for skin hydration monitoring," *Sensors*, vol. 22, no. 18, 2022.

[27] S. Anastasova, P. Kassanos, and G. . Yang, *Electrochemical sensor designs for biomedical implants*, pp. 19–98. Implantable Sensors and Systems: From Theory to Practice, 2018.

[28] L. Iannucci, M. Parvis, P. Cristiani, R. Ferrero, E. Angelini, and S. Grassini, "A novel approach for microbial corrosion assessment," *IEEE Transactions on Instrumentation and Measurement*, vol. 68, no. 5, pp. 1424–1431, 2019.

[29] G. Soliveri, V. Pifferi, G. Panzarasa, S. Ardizzone, G. Cappelletti, D. Meroni, K. Sparnacci, and L. Falciola, "Self-cleaning properties in engineered sensors for dopamine electroanalytical detection," *Analyst*, vol. 140, no. 5, pp. 1486–1494, 2015.

[30] L. Iannucci, "Chemometrics for data interpretation: Application of principal components analysis (pca) to multivariate spectroscopic measurements," *IEEE Instrumentation and Measurement Magazine*, vol. 24, no. 4, pp. 42–48, 2021.

[31] Q. Yan, X. Liao, C. Zhang, Y. Zhang, S. Luo, and D. Zhang, "Intelligent monitoring and assessment on early-age hydration and setting of cement mortar through an emi-integrated neural network," *Measurement: Journal of the International Measurement Confederation*, vol. 203, 2022.

[32] K. Zhang, J. Wang, T. Liu, Y. Luo, X. J. Loh, and X. Chen, "Machine learning-reinforced noninvasive biosensors for healthcare," *Advanced Healthcare Materials*, vol. 10, no. 17, 2021.